Research Article | Vol. 29, No. 14 / 5 July 2021 / Optics Express 22159
Optics EXPRESS

Shear based gap control in 2D photonic quasicrystals of dielectric cylinders

ÁNGEL ANDUEZA,[1,2,*] JOAQUÍN SEVILLA,[1,2] JESÚS PÉREZ-CONDE,[3,4] AND KANG WANG[5]

[1]Dpto. Ing. Eléctrica, Electrónica y Comunicación, Universidad Publica de Navarra, 31006 Pamplona, Spain
[2]Institute of Smart Cities (ISC), Universidad Publica de Navarra, 31006 Pamplona, Spain
[3]Dpto. de Ciencias, Universidad Publica de Navarra, 31006 Pamplona, Spain
[4]Institute for Advanced Materials (INAMAT), Universidad Publica de Navarra, 31006 Pamplona, Spain
[5]Laboratoire de Physique des Solides, CNRS, Université Paris-Saclay, 91405 Orsay, France
*angel.andueza@unavarra.es

Abstract: 2D dielectric photonic quasicrystals can be designed to show isotropic band gaps. In this work we study a quasiperiodic lattice made of silicon dielectric cylinders ($\varepsilon = 12$) arranged as periodic unit cell based on a decagonal approximant of a quasiperiodic Penrose lattice. We analyze the bulk properties of the resulting lattice as well as the bright states excited in the gap, which correspond to localized resonances of the electromagnetic field in specific cylinder clusters of the lattice. Then we introduce a controlled shear deformation γ which breaks the decagonal symmetry and evaluate the width reduction of the gap together with the evolution of the resonances, for all shear values compatible with physical constraints (cylinder contact). The gap width reduction reaches 18.5% while different states change their frequency in several ways. Realistic analysis of the actual transmission of the electromagnetic radiation, often missing in the literature, has been performed for a finite "slice" of the proposed quasicrystals structure. Two calculation procedures based on MIT Photonic Bands (MPB) and Finite Integration Technique (FIT) are used for the bulk and the finite structures showing an excellent agreement between them.

1. Introduction

Photonic band gap (PBG) materials have been investigated for more than three decades since the germinal paper of Ohtaka [1,2]. One of the main objectives of the past PBG effort was the search of metamaterials with new optical related properties like isotropic band gap [3], zero-refractive index [4], slow light manipulation [2], etc. These PBG allow creating waveguides [5], sensors [6], collimators [7] or to improve the existent solar cells [8], etc. Some realistic PBG materials were early proposed in three [9] and two dimensions [10,11] based on periodic lattices with complete but anisotropic band gaps (see for instance Ref. [12], specially chapter 5 for 2D Photonic Crystals). Isotropic band gaps are preferred, though, for some applications such as wavelength selective mirror or filters [13] slow light technology [14], filters [15], collimators [7] or band filters [15]. On the other hand, all-dielectric photonic crystals do not contain metallic elements and therefore can be fabricated with only dielectric components [16,17]. Meta-optics based in Mie-type resonances in all-dielectric nanostructures is an emerging field [17]. The creation of photonic materials with complete band gap is also important to control spontaneous emission and Purcell effect [17]. All-dielectric photonic quasicrystals can be also viewed as bandgap systems [18–20] or as zero-refractive index homogeneous materials [4].

Photonic quasicrystals (PQC) have been proposed and built with dielectric cylinders [21,22]. Some of these structures presented an almost isotropic band gap which is one of the required features to build most of the applications. Since then many QC structures based on dielectric

#427235 https://doi.org/10.1364/OE.427235
Journal © 2021 Received 9 Apr 2021; revised 2 Jun 2021; accepted 3 Jun 2021; published 29 Jun 2021

Optics EXPRESS

cylinders have been investigated [5,18,20,23,24]. In these works high permittivity contrast (cylinder vs surrounding material) was needed to get a complete and sizable band gap as it was in periodic two dimensional Photonic Crystal (PC) case [2]. Recently, low refractive index contrast 1.6:1 PBG's based on hyperuniform 2D structures have been also investigated [3] and demonstrated the possibility to build PBG with low/medium refractive indexes. Quasiperiodic arrays have also been proven very interesting in plasmonics [25] especially for broadband, polarization independent transmission enhancement [26], working in a similar way to the photonic materials with complete bandgaps.

An important issue with PBG and PQC in particular, is to create a device with a gap which could be also modified in controlled way. We propose here a way to create such structures, which show an almost isotropic gap, that can be also controlled with only geometrical parameters. We study a configuration of silicon cylinders ($\varepsilon = 12$) arranged in a (regular) lattice of Penrose quasicrystal approximants, a generalization of the previously analyzed case in Ref. [19]. In previous studies it has been shown the onset of states in the gap due to Mie-like localized resonances [18,19,24]. These resonances were reported within a band structure but without a description of their actual transmission properties. Here we calculate their transmission output and their evolution with the shear of the underlying lattice, together with the band structure of the corresponding bulk lattice. We also analyze the group velocity of these resonances, which is very small [18], an important feature for applications where slow light technology is needed [2].

Finally, the simulations have been realized assuming that the cylinders are surrounded by air, although the results should remain valid for cylinders in a dielectric matrix if the permittivity contrast is kept.

2. System under study and calculation procedures

We want to study the effect of symmetry breaking by shear in the gap of photonic quasicrystals and, at the same time, we analyze how this variation affects light transmission through the material. The gap calculations are performed on an infinite periodical system, while the transmission data must be obtained from a sample of finite dimension in the direction of light transmission. The size effects of the quasicrystal width are also analyzed in the calculations.

In the following subsections we describe how both systems are built (2.1), how shear is applied (2.2) and the numerical methods used for the calculations (2.3): MIT Photonic Band (MPB) for photonic band gap and Finite Integration Technique (FIT) implemented by CST Microwave studio for transmission calculations.

2.1. Quasicrystal approximants and Bravais lattices

The bulk quasicrystal photonic lattices are not suitable to build a physical realization nor to perform transmission calculations on them. In this work we define approximants of the parent QC as the unit cell of an otherwise periodic lattice as was first proposed in Ref. [22]. The approximant-based lattice reproduces most of the properties of the parent QC lattice, such as tenfold rotational symmetries, long-range decagonal bond-orientational symmetries and photonic band gap. In addition, it allows to use the standard computational methods developed for periodic photonic crystals (see Fig. 1).

As far as transmission computations are concerned, we need a lattice which is finite in the propagation direction to obtain a sizable output. As the signal intensity decreases with the lattice width, we must arrive to a compromise between contrast, gap and resonant states intensity, which needs a big enough crystal, and a measurable transmission. On the other hand, we know that at least three wavelength wide width in the propagation direction is necessary to get an adequate contrast between the in-gap states and the gap background in the previous work [6].

Optics EXPRESS

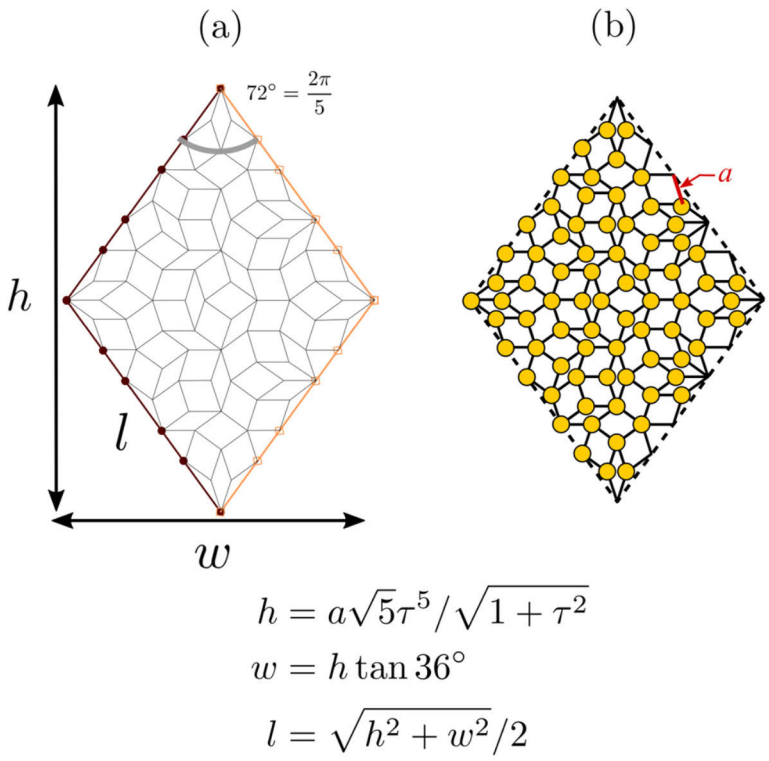

Fig. 1. (a) Decagonal approximant in the original QC. (b) The unit cell is delimited by dashed and the lattice nodes are highlighted by yellow circles and correspond to dielectric cylinders.

The decagonal approximant produces an oblique $2\pi/5$ rhombus-shaped Bravais lattice (see Fig. 1) and needs a more complex procedure for the transmission simulations. CST allows only to define orthogonal bases, so we had to adapt the decagonal oblique approximant to this constraint.

The procedure to get a unit cell adapted to a rectangular basis is as follows. We added to the original rhombus four triangles in order to complete a rectangle as shown in Fig. 2(b). From this cell we can easily create an ordinary rectangular Bravais lattice where each lattice point contains now 152 cylinders, as shown in Fig. 2(b). The original approximant width was $w = a\sqrt{5}\tau^3$ and height $h = a\sqrt{5}\tau^5/\sqrt{1+\tau^2}$, where a is the edge length of the tiles that build up the decagonal approximant employed and τ is the golden number. The rod radius considered is $r = 0.25$ a.

The new rectangular unit size is correspondingly $w \times h$ as shown in Fig. 2(b). The size of the lattice in the propagation direction, h, is wide enough to meet the previous requirements of contrast between gap and in-gap states and, on the other hand, it is thin enough to allow transmission measurements [6]. The final approximant shapes and sizes used with CST technique are depicted in Fig. 2(c). The band structure, though, is calculated as a whole 2D lattice with the MPB package [27] with the rhombus unit cell containing 76 rods as shown in Fig. 2(a).

2.2. *Broken rotational symmetry by shear*

We investigate the behaviors of the samples as we shear the sample lattice, in which the local decagonal rotational symmetry is broken, while the circular shape of the dielectric rods remain unmodified. Shear is one of the three possible transformations that can be applied to a lattice. A generic strain or deformation, **D**, in two dimensions can be implemented with a deformation

Optics EXPRESS

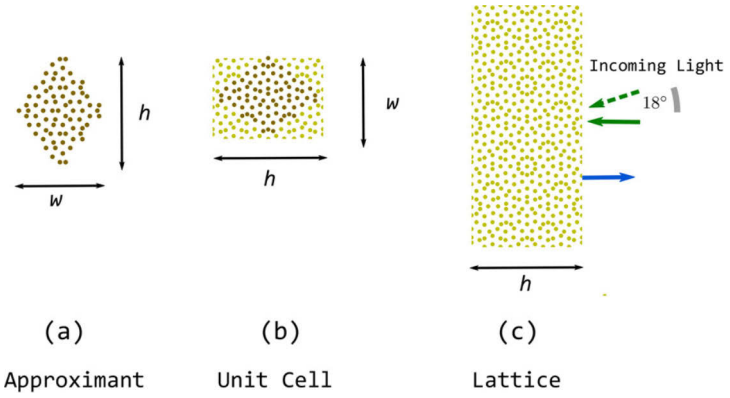

Fig. 2. Approximant and unit cells for decagonal approximant (brown) and computational sized $h \times w$ cell used in transmission CST calculations. The specific values of h, w, r are also given, where $r = 0.25$ a is the cylinder radius. Blue arrows are the normal to the QC surface and green arrows indicate the range of possible different incoming light directions.

applied to every (x, y) point, so that the new transformed point (x', y') can be written as [28],

$$\begin{pmatrix} x' \\ y' \end{pmatrix} = \mathbf{D} \cdot \begin{pmatrix} x \\ y \end{pmatrix} = \begin{pmatrix} a & b \\ c & d \end{pmatrix} \cdot \begin{pmatrix} x \\ y \end{pmatrix} = \begin{pmatrix} ax + by \\ cx + dy \end{pmatrix}. \tag{1}$$

Any lattice deformation, **D**, can be decomposed in a dilatation, a rotation and a shear. We are interested in deformations that can modify the band structure or the lattice transmission spectrum. Also, although global dilatation do produce a shift of the whole spectra, and it could be thought as a modification, this behavior can be also seen as a simple scaling of the lengths and frequencies in the Maxwell equations and no symmetry change is implied. We therefore restrict the possible deformations to those of pure shear which break the rotational n-fold symmetry of the QC. The shear transformations, **S**, can be described by the matrix,

$$\mathbf{S} = \begin{pmatrix} 1 & \gamma_x \\ \gamma_y & 1 \end{pmatrix}. \tag{2}$$

where γ_x, γ_y are two real numbers which reflect the amount of the shear in the x, y directions respectively. The transformed points (x', y') from (x, y) are given from Eq. (1),

$$\begin{pmatrix} x' \\ y' \end{pmatrix} = \begin{pmatrix} 1 & \gamma_x \\ \gamma_y & 1 \end{pmatrix} \cdot \begin{pmatrix} x \\ y \end{pmatrix} = \begin{pmatrix} x + y\gamma_x \\ y + x\gamma_y \end{pmatrix}. \tag{3}$$

After several preliminary tests, we found no relevant differences in the independent variation of shear in x and y directions regarding mutual variation, therefore, for simplicity, from now on we restrict our study to shear transformations with the same deformation in both axes, $\gamma_x = \gamma_y = \gamma$, so that we only need γ parameter to characterize a given shear. In Fig. 3 the effects of the shear for the decagonal approximant are shown, together with the corresponding original and sheared Bravais lattices. The angles α and β are measured from y-axis to the primitive vectors $\mathbf{a}_1$ and $\mathbf{a}_2$, therefore, are transformed by shear. The new angles are labeled α_{sh} and β_{sh}.

As the shear is applied to the whole quasicrystal, the approximants are transformed and the corresponding Bravais lattices are also modified as was shown in Fig. 3. We need to calculate

Optics EXPRESS

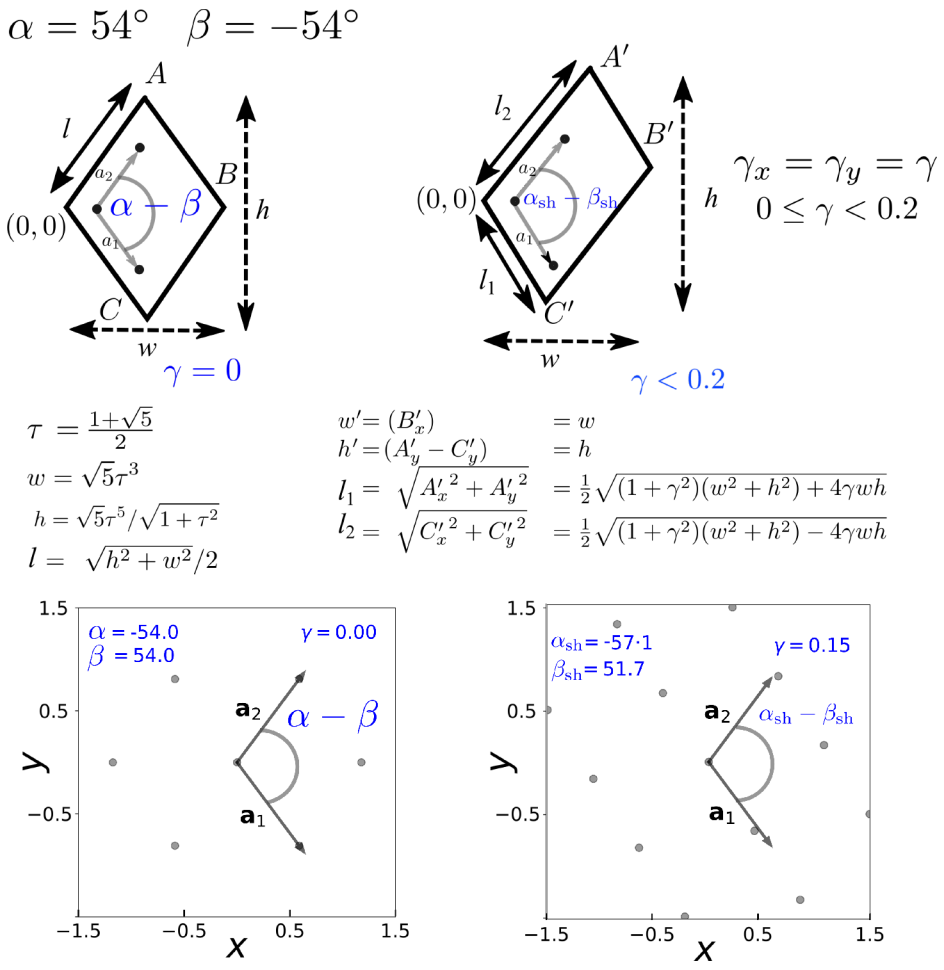

Fig. 3. Unit cells of decagonal approximants in the original QC and in the sheared case used with the MPB technique (top). And the Bravais lattice of the approximant for the shear values $\gamma = 0.0$ and $\gamma = 0.15$, respectively. The angles α and β are measured from the y-axis to the primitive vectors $\mathbf{a}_1$ and $\mathbf{a}_2$

Optics EXPRESS

the new sheared Brillouin zones (BZ), their irreducible part and the special symmetry points to compute the bands at these special values. In Fig. 4 we show the original oblique Brillouin zone from decagonal approximant at $\gamma = 0$. We also illustrate the cases for $\gamma \neq 0$ with two values of γ, 0.05 and 0.15, respectively. The loss of symmetry in these cases is clearly seen as the irreducible BZ of the sheared lattice is half of the whole BZ, whereas the original unsheared irreducible BZ's for the decagonal lattice was one fourth of the whole BZ. This is the expected behavior for the irreducible BZ: its size is always the one $g-$th part of the first Brillouin zone (see Ref. [29] p. 281). Here g is the number of symmetry operations of the original point group: C_{2v}, $g = 4$ of the not sheared oblique periodic lattice and C_1, $g = 2$ of the sheared oblique case.

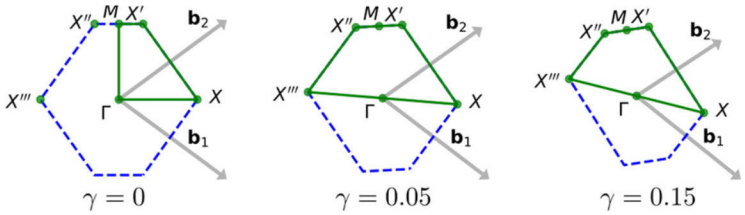

Fig. 4. Brillouin zone of the approximant-based Bravais lattice (dashed blue line) together with the irreducible BZ (green) for three values of $\gamma = 0, 0.05$ and 0.15. The irreducible BZ is one fourth of the BZ for $\gamma = 0$, but when the rotational symmetry is broken, $\gamma \neq 0$, it is half of the BZ. The primitive vectors of the reciprocal lattice, $\mathbf{b}_1$ and $\mathbf{b}_2$, are also shown.

2.3. Numerical methods

We compute the periodic approximant-based lattices band by means of preconditioned conjugate-gradient minimization of the block Rayleigh quotient in a plane-wave basis, using MIT Photonic Bands package [27]. The MPB software allows inspecting in detail the band structure, gap and resonant in-gap states due to light localization. Those quantities describe a periodic and therefore infinite lattice, however, in actual applications, we need to address the experimental accessibility of the photonic lattice, in particular the transmission properties in a finite sample. We investigate this issue by means of FIT [30,31] with the CST MICROWAVE STUDIO^{TM}, a commercial code. The use of both methods allows, additionally, to cross-checking the results.

The numerical simulations for a finite version are performed on a two dimensional lattice of dielectric cylinders infinite in the y direction and assuming infinite length cylinders in the x direction (infinite length rods). The incoming radiation travels in the z direction as Transverse Electric and Magnetic (TEM) mode with the electric field along the x-axis and the magnetic field along the y-axis. The incoming wave presents an incidence angle φ of 18° to the external surface of the structure as is indicated by the dashed green arrow in Fig. 2(c). A frequency solver tool with a tetrahedral adaptive mesh refinement was used to calculate the power balance of the PQC in CST. The symmetry of the finite PQC and the orientation of the electromagnetic field allow us to simplify the problem by restricting the calculation to a rectangular unit cell. CST solves the Maxwell equations and analyzes the weight of each diffraction order separately. A summation of the power density in all diffraction orders provides the total reflectance, R, and transmittance, T. As the refractive index employed for the calculations is real, the absorptivity of the QC is not considered in the power balance.

3. Results and discussion

We calculate the transmission spectra with the CST for different lattice widths in the z direction, starting with the largest case (h wide) as depicted in Fig. 2(b). Then, row after row, the cylinders are removed and the resulting transmission obtained for each width value. A total of 15

Optics EXPRESS

configurations are obtained in the process. The gap and resonances frequencies are then obtained from the analysis of the resulting spectra. The bulk counterpart, as a periodic lattice of decagonal approximants is shown in Fig. 2(c) for the original (unsheared) and sheared lattices, is analyzed with the MPB package. We obtain the first 110 bands, which are enough to capture the whole gap frequency range as well as the resonant states in the gap interval.

Results are presented in Fig. 5, 6 and 7 for the values of shear $\gamma = 0$, 0.05 and 0.1 respectively. The three figures have the same structure, composed of different images that summarize all results. In the top left corner (labeled by a) there is a color map that presents the transmission spectra (hotter colors higher transmission) for different widths of the sample along the horizontal axis. Frequency is presented normalized to the lattice parameter a along the vertical axis (see Fig. 1). Sample width, presented as h/a, is also normalized to the same dimensional parameter. This representation is made by adding several spectra as the one shown in the top right figure (labeled by c) calculated with CST for different values of sample width and interpolating to get a smoother color plot. The onset of a well-defined gap as width increases can clearly be seen in this representation. In addition, several bright states inside the gap are clearly observable.

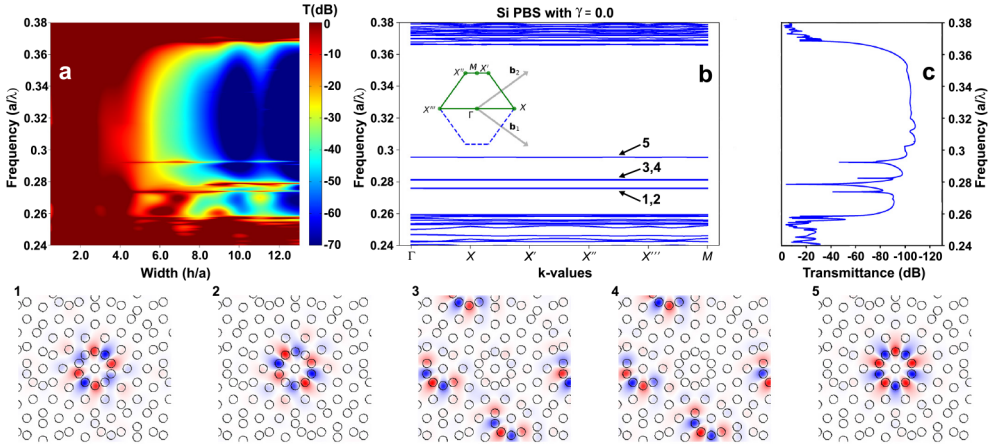

Fig. 5. Original lattice, $\gamma = 0$. (a) Transmission spectra dependence on the normalized width, h/a (top left color map). (b) Band of the bulk lattice in the same frequency interval, around the gap (top center). The five resonances in the gap are labeled and their field distribution show below. (c) The transmission spectrum for the widest lattice is also shown $h/a = 13$ (top right).

The band structure of the corresponding bulk lattice, calculated with MPB, is shown in the figures at top center (labeled by "b"), in the same frequency interval as the transmission data, so that comparisons between the two calculations can be readily made. The frequencies of gap edges and resonant states, within the gap for the bulk structure, are very close to those observed in the transmission spectra for a finite sample (simulated with CST). We also show the electric field intensity distribution of the 5 bright states as identified in the bulk lattice band calculations (numbers 1 to 5 in the lower part of the figure). These data are calculated with MPB and presented normalized to ±1 (red and blue) in all cases.

In the three cases studied here, the MPB calculations of the bulk lattice and the CST simulations of finite samples are in excellent agreement. Concordance is particularly good in the first two cases, while for $\gamma = 0.1$ a slight mismatch in the frequency position for state 5 can be appreciated. Gap evolution with thickness can be seen in Figs. 5(a), 6(a) and 7(a). The general behavior is similar in the three cases. We observe that, for small thickness, attenuation is scarce at all frequencies and there is no contrast indicating a gap. A depression in transmission indicating

Optics EXPRESS

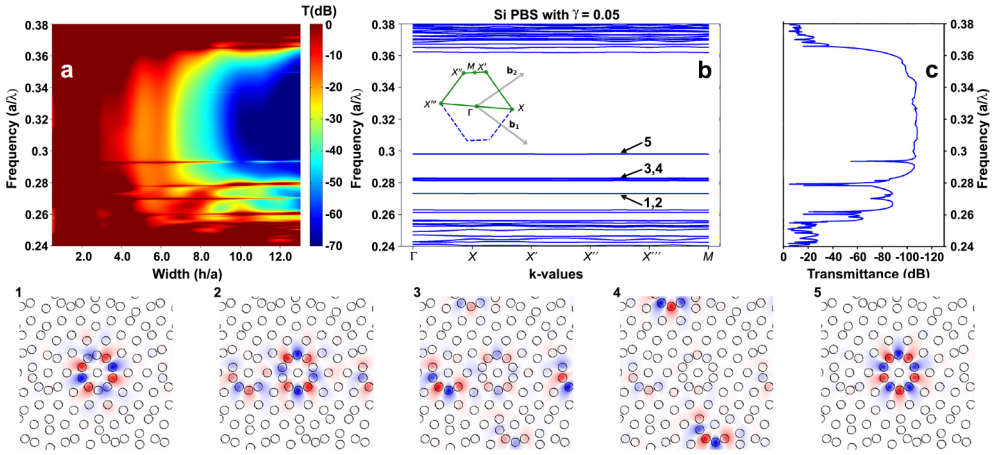

Fig. 6. Sheared lattice $\gamma = 0.05$. The same quantities as in Fig. 5.

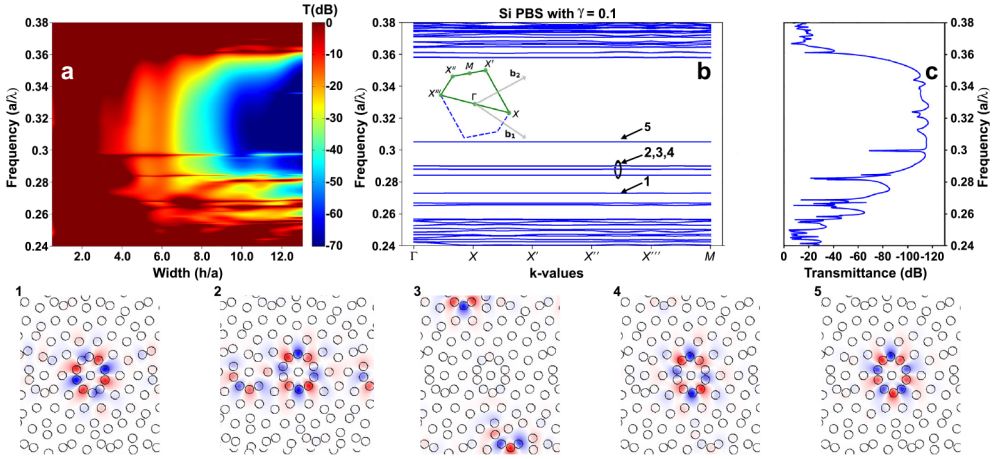

Fig. 7. Sheared lattice $\gamma = 0.1$. The same quantities as in Fig. 5.

the gap existence starts to be noticeable for widths from 3 to 6. For the central frequencies, the transmission keeps diminishing while the transmission values out of the gap remain quite high. The maximum contrast between gap and its borders is attained for $h/a = 8$.

The gap range decreases with lattice deformation, presenting a gap width reduction of 18.5% for $\gamma = 0.1$. The frequency range of low transmission is smaller as the shear increases. This happens because both gap borders move towards the center for higher values of shear. This can be seen by comparing the representations of transmission and band structures in Figs. 5, 6 and 7. The former (5(b), 6(b) and 7(b)), suggest that several bands that are packed near the gap edges for the undisturbed lattice begin to open and lose degeneration when QC symmetry starts to vanish due to deformation. In Fig. 8 we provide smooth curves of the evolution of the gap edges with shear, calculated for much more values of shear than those shown in previous figures.

It is interesting to note that the bands inside the gap are significantly flatter than the bands present near the edge of the band gap. This characteristic shows that the light propagates very slowly at the frequency of the excited states due to the slowing down of group velocity [24].

Optics EXPRESS

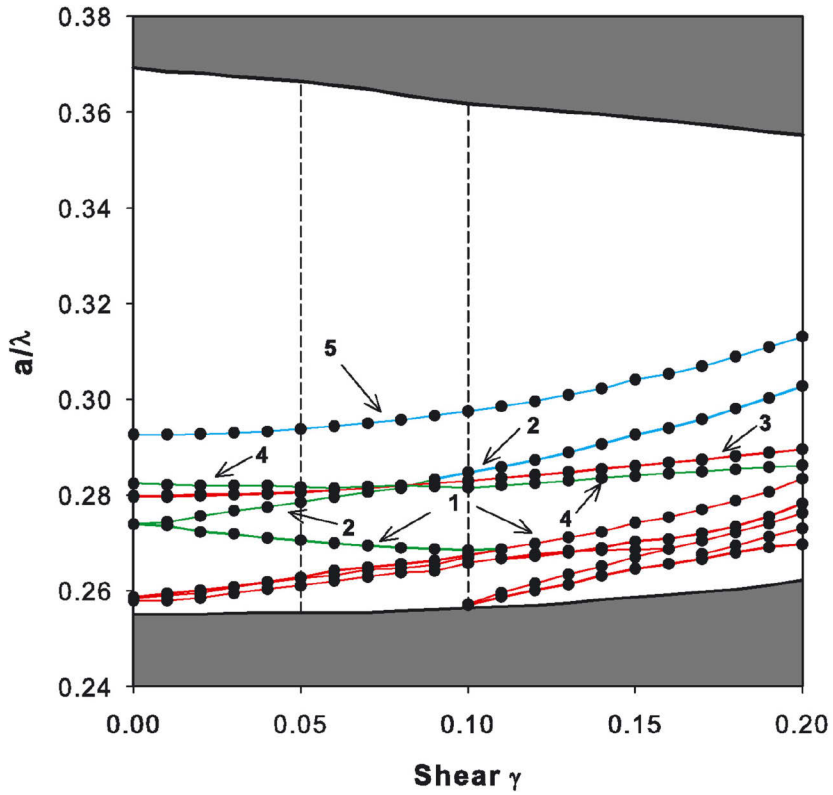

Fig. 8. Frequency evolution of the resonances width shear for $h/a = 13$ with. Resonances are labelled from 1 to 5 keeping the same tags as in previous figures. The edges of the bandgap are represented by the gray area. The vertical dashed lines indicate the shear values presented in detail in Figs. 6 and 7. The colors of the lines indicate the intensity of the resonance in the transmission spectra: red for high from 0 to -20 dB, green for medium, from -20 to -40 dB and blue for the weaker ones, lower than -40 dB.

This confirms that the low group velocity is essentially related to the resonant states on the local decagonal rings of the lattice and other cylinder clusters, even when shear disturbs the lattice.

Bright states inside the gap can be clearly seen in Figs. 5, 6 and 7. The states are present in the band structure (shown as "b" in the three figures) and are also visible at frequencies of high transmission in the color maps (labelled a in the figures) presenting a significant good match. These states are due to local resonances of a cylinder clusters of the structure as shown in the lower part of Figs. 5 to 6 and 7. The states are labeled 1 through 5 in accordance with their naming in the band structure. Resonance labelled 5 corresponds to a full symmetric resonance of the decagonal ring in the center of the structure, with five maxima and five minima placed in each cylinder of the ring. Resonances 1 and 2 are also held in the decagonal ring but are composed of only four maxima and minima, not fitting so well with the cylinders and allowing two configurations (rotated from each other). These two geometrical configurations are totally equivalent and therefore their frequency values are the same, appearing degenerate in the band structure of the undisturbed lattice (Fig. 5). However, this degeneration is lifted when shear is introduced, and the local symmetry is broken.

Resonances 3 and 4 are due to incomplete decagonal rings ("C" shaped half ring), apart from the decagonal ring. Two families of incomplete rings deform differently when shear is introduced, separating their frequency values that were degenerated in the undisturbed lattice. However,

Optics EXPRESS

these two geometrical configurations remain very similar, so their frequency is quite close. There are other possible resonant configurations of substructures of the lattice (close to the edge of the gap), but their frequency lies outside the bandgap and cannot be considered as isolated states.

As we mentioned above, the states in the gap appear as high transmission frequencies in the spectrum (Figs. 5(a), 6(a) and 7(a)). When radiation in open space reaches the edge of a finite sample of the structure, it excites the resonance of the cylinder clusters for the appropriate frequencies. This excitation is transmitted from cluster to cluster until the other side of the sample is reached and the sample radiates again to the free space. Therefore, the radiation is able to excite resonances and can traverse the sample end to end, metaphorically jumping in the clusters, in the same way that a person can cross a river jumping from stone to stone. This is the reason why the transmission at the frequency of the states remains high as the sample width is increased, while the one of other frequencies decreases much more quickly. This generates a significant contrast between the transmission of the states and its background for widths bigger than h/a=4. A study of the optimum width to improve contrast in this kind of systems was published elsewhere [6].

In order to follow closely the evolution of the states in the gap with shear, we calculated the transmission of samples of additional deformation values that those presented previously as Figs. 5(c), 6(b) and 7(c). In all cases the calculations are performed on finite samples wide enough to have the gap fully developed (h/a = 13). The results are presented in Fig. 8.

There are many interesting features than can be derived from this figure, such as the decrease in the gap width (mainly reduced by the decreasing of the upper edge) or the increase in the number of modes that appear as deformation rises (mainly departing from the lower gap edge).

Most of the states excited inside the band gap show a strong dependence on shear, increasing their frequency position with it. Exceptions are states 3 and 4 (that remain unaltered for certain intervals) and state 1, the only that decreases in frequency. The different slopes of these curves lead to crossings as the one observed for shear around 0.08, where states 2, 3 and 4 change their relative positions. States 1 and 2, degenerate in the unaltered system, quickly diverge in opposite directions for low values of shear. The initial frequency decrease of state 1 ends for a shear value of 0.1, and from this point on, merges with other states that rise in frequency. It is important to note that some of these states, especially states 1, 2 and 3, are quite bright, and present a significant contrast with respect to the background, that could lead to interesting applications. We have explored elsewhere [32] the possible construction of a strain sensor based on the frequency difference between states 1 and 2.

4. Conclusion

We have studied the effect of shear in the photonic band structure and transmission properties of 2D dielectric photonic quasicrystals based on cylinders with high dielectric permittivity (ε = 12). The band structure of the bulk lattice (and field distribution of the resonances) was calculated with MPB, while the transmission of finite samples of different widths was calculated with CST software. The system presents an isotropic bandgap and five bright states inside the gap. These features can be observed (with a remarkable match) in both, the finite sample transmission and in the bulk photonic band structure. The photonic states in the bandgap are due to Mie-like resonances of local clusters of cylinders and are associated with very flat bands, which generates very low group velocity of the transmitted radiation. The quasicrystal undergoes a remarkable electromagnetic response shear-induced variation, gap bandwidth decreases (18.5% for γ = 0.1), and the distortion of the position of the cylinders, breaks frequency degeneration of excited states into the bandgap and shifts the frequency values of all of them. Besides, we observe a complex evolution of the frequency position of the states with shear. This set of characteristics is interesting in the design of practical devices such as sensors.

Disclosures. The authors declare that there are no conflicts of interest related to this article.

Optics EXPRESS

Data availability. Data underlying the results presented in this paper are not publicly available at this time but may be obtained from the authors under request.

References

1. K. Ohtaka, "Energy band of photons and low-energy photon diffraction," Phys. Rev. B **19**(10), 5057–5067 (1979).
2. M. Notomi, "Manipulating light with strongly modulated photonic crystals," Rep. Prog. Phys. **73**(9), 096501 (2010).
3. W. Man, M. Florescu, K. Matsuyama, P. Yadak, G. Nahal, S. Hashemizad, E. Williamson, P. Steinhardt, S. Torquato, and P. Chaikin, "Photonic band gap in isotropic hyperuniform disordered solids with low dielectric contrast," Opt. Express **21**(17), 19972–19981 (2013).
4. S. V. Boriskina, "Quasicrystals: Making invisible materials," Nat. Photonics **9**(7), 422–424 (2015).
5. T. PriyaRose, G. Zito, E. Di Gennaro, G. Abbate, and A. Andreone, "Control of the light transmission through a quasiperiodic waveguide," Opt. Express **20**(23), 26056–26061 (2012).
6. A. Andueza, K. Wang, J. Pérez-Conde, and J. Sevilla, "Optimal width of quasicrystalline slabs of dielectric cylinders to microwave radiation transmission contrast," J. Appl. Phys. **120**(8), 083101 (2016).
7. A. F. Matthews, "Experimental demonstration of self-collimation beaming and splitting in photonic crystals at microwave frequencies," Opt. Commun. **282**(9), 1789–1792 (2009).
8. I. Cornago, S. Dominguez, M. Ezquer, M. J. Rodríguez, A. R. Lagunas, J. Pérez-Conde, R. Rodriguez, and J. Bravo, "Periodic nanostructures on unpolished substrates and their integration in solar cells," Nanotechnology **26**(9), 095301 (2015).
9. E. Yablonovitch and T. J. Gmitter, "Photonic band structure: The face-centered-cubic case," Phys. Rev. Lett. **63**(18), 1950–1953 (1989).
10. P. R. Villeneuve and M. Piché, "Photonic band gaps in two-dimensional square lattices: Square and circular rods," Phys. Rev. B **46**(8), 4969–4972 (1992).
11. R. D. Meade, K. D. Brommer, A. M. Rappe, and J. D. Joannopoulos, "Existence of a photonic band gap in two dimensions," Appl. Phys. Lett. **61**(4), 495–497 (1992).
12. J. D. Joannopoulos, S. G. Johnson, J. N. Winn, and R. D. Meade, *Photonic Crystals: Molding the Flow of Light* (Princeton University, 2008).
13. K. Edagawa, "Photonic crystals, amorphous materials, and quasicrystals," Sci. Technol. Adv. Mater. **15**(3), 034805 (2014).
14. T. Baba, "Slow light in photonic crystals," Nat. Photonics **2**(8), 465–473 (2008).
15. N. B. Ali and M. Kanzari, "Designing of stop band filters using hybrid periodic/quasi-periodic one-dimensional photonic crystals in microwave domain," Phys. Status Solidi **208**(1), 161–171 (2011).
16. K. Edagawa, "All-dielectric metamaterials," Nat. Nanotechnol. **11**(1), 23–36 (2016).
17. I. Staude, T. Pertsch, and Y. S. Kivshar, "All-Dielectric Resonant Meta-Optics Lightens up," ACS Photonics **6**(4), 802–814 (2019).
18. K. Wang, "Structural effects on light wave behavior in quasiperiodic regular and decagonal Penrose-tiling dielectric media: A comparative study," Phys. Rev. B **76**(8), 085107 (2007).
19. K. Wang, "Light localization in photonic band gaps of quasiperiodic dielectric structures," Phys. Rev. B **82**(4), 045119 (2010).
20. Z. V. Vardeny, A. Nahata, and A. Agrawal, "Optics of photonic quasicrystals," Nat. Photonics **7**(3), 177–187 (2013).
21. M. E. Zoorob, M. D. B. Charlton, G. J. Parker, J. J. Baumberg, and M. C. Netti, "Complete photonic bandgaps in 12-fold symmetric quasicrystals," Nature **404**(6779), 740–743 (2000).
22. K. Wang, S. David, A. Chelnokov, and J. M. Lourtioz, "Photonic band gaps in quasicrystal-related approximant structures," J. Mod. Opt. **50**(13), 2095–2105 (2003).
23. J. Romero-Vivas, D. Chigrin, A. Lavrinenko, and C. Sotomayor Torres, "Resonant add-drop filter based on a photonic quasicrystal," Opt. Express **13**(3), 826–835 (2005).
24. K. Wang, "Light wave states in two-dimensional quasiperiodic media," Phys. Rev. B **73**(23), 235122 (2006).
25. V. G. Achanta, "Plasmonic quasicrystals," Prog. Quantum Electron. **39**, 1–23 (2015).
26. S. Kasture, A. P. Ravishankar, V. J. Yallapragada, R. Patil, N. V. Valappil, G. Mulay, and V. G. Achanta, "Plasmonic quasicrystals with broadband transmission enhancement," Sci. Rep. **4**(1), 5257 (2015).
27. S. Johnson and J. Joannopoulos, "Block-iterative frequency-domain methods for Maxwell's equations in a planewave basis," Opt. Express **8**(3), 173–190 (2001).
28. R. W. Ogden, *Non-Linear Elastic Deformations* (Dover Publications, 1997).
29. A. W. Joshi, *Elements of Group Theory for Physicists* (New Age International, 1997).
30. M. Clemens and T. Weiland, "Discrete electromagnetism with the finite integration technique," Prog. Electromagn. Res. **32**, 65–87 (2001).
31. T. Weiland, "Finite integration method and discrete electromagnetism," in *Computational Electromagnetics*, (Springer, 2003), pp. 183–198.
32. A. Andueza, J. Pérez-Conde, and J. Sevilla, "Strain sensing based on resonant states in 2d dielectric photonic quasicrystals," Opt. Express **29**(5), 6980–6990 (2021).